# scientific reports

OPEN

# Geodetic monitoring of the recent activity and the dome forming eruption at Nevado del Ruiz (Colombia), 2010–2023

Milton Ordoñez[1✉], Juan Idárraga[1], Roberta Adamo[2] & Maurizio Battaglia[2,3]

**Nevado del Ruiz (Colombia) is infamous for the catastrophic eruption of 1985 that destroyed the villages of Armero and Chinchiná. However, this was not the volcano's first destructive event; similar eruptions also occurred in 1595 and 1845. In 1985, the limited geodetic data available failed to provide a clear warning of the impending eruption. Since then, advancement in geodetic monitoring, now incorporating tilt and satellite geodesy, along with improvements in seismic, geochemical, geological and remote sensing monitoring, have enhanced hazards assessment and mitigated the risk during subsequent eruptions in 1989, 2012, and 2015–2019, as well as during periods of unrest over the last 13 years. Modeling of deformation data over the past 13 years reveals complex interactions between the local, shallow magmatic system beneath Nevado del Ruiz and a deep, regional magmatic system beneath Nevado de Santa Isabel, 9 km southwest of Nevado del Ruiz. Before February 2012, the volcano deflated because of the depressurization of the local shallow reservoir. This same reservoir later fueled ash emissions and gas release (2012–2023), and a dome-forming eruption (2015–2019). In contrast, the inflation observed from 2012 to 2023 is linked to the pressurization of the deep reservoir beneath the Nevado de Santa Isabel.**

Nevado del Ruiz is an andesite-dacitic stratovolcano in the Central Cordillera of Colombia (Fig. 1b), and one of the most active volcanoes of Colombia. It is one of the volcanoes of the Nevado del Ruiz Volcanic Complex[1] and part of the North Volcanic Segment of Colombia, a group of 12 volcanoes aligned N–S and extending for 137 km along the highest part of the Central Cordillera (Fig. 1c). The Volcanic Complex has a calk-alkaline volcanism of active continental andesite margin type with dacitic and andesitic lava and pyroclastic flows, pyroclastic debris, and lahar deposits[1]. It also hosts a sizeable hydrothermal system, inferred from several hot springs found in its vicinity[2]. The summit of Nevado del Ruiz is flat and covered by an ice cap of about 9 km[2][3].

The paroxysmal explosive eruption of November 13th, 1985 (VEI = 4) deposited a large amount of pyroclastic material in the Arenas crater that led to the sudden melting of the volcano ice cap, and the formation of a large-volume lahar that reached and destroyed the town of Armero and some neighborhoods of the town of Chinchiná, causing approximately 25,000 fatalities[4]. The volcano experienced several small eruptions between 1985 and 1991[5], with a second paroxysmal explosive eruption in 1989. However, this eruption did not result in any fatalities[6]. Two small explosive eruptions (VEI = 1) occurred on May 29th and June 30th, 2012, generating small lahars confined to the proximal area of the volcano. The last effusive eruption of Nevado del Ruiz began in September 2015, leading to the emplacement of a lava dome at the bottom of the main crater[3]. Between 2012 and 2023, hundreds of small explosions and ash emissions took place, resulting in minor deposition of pyroclastic material.

Since 1985, the geodetic monitoring of Nevado del Ruiz has evolved into a system that incorporates tilt, Global Navigation Satellite System (GNSS) and Interferometric Synthetic Aperture Radar (InSAR;[8]) (Fig. 1). Geodetic monitoring, integrated with seismic[5], geochemical, geological, remote sensing, and ground-based infrasound monitoring[9] has allowed the Colombian Geological Survey to better understand the behavior of the volcano,

[1]Colombian Geological Survey, Volcanological and Seismological Observatory of Manizales, 170001 Caldas, Manizales, Colombia. [2]Department of Earth Sciences, Sapienza – University of Rome, 00185 Rome, Italy. [3]U.S. Geological Survey, Volcano Disaster Assistance Program, Moffet Field, CA 94035, USA. ✉email: mordonez@sgc.gov.co
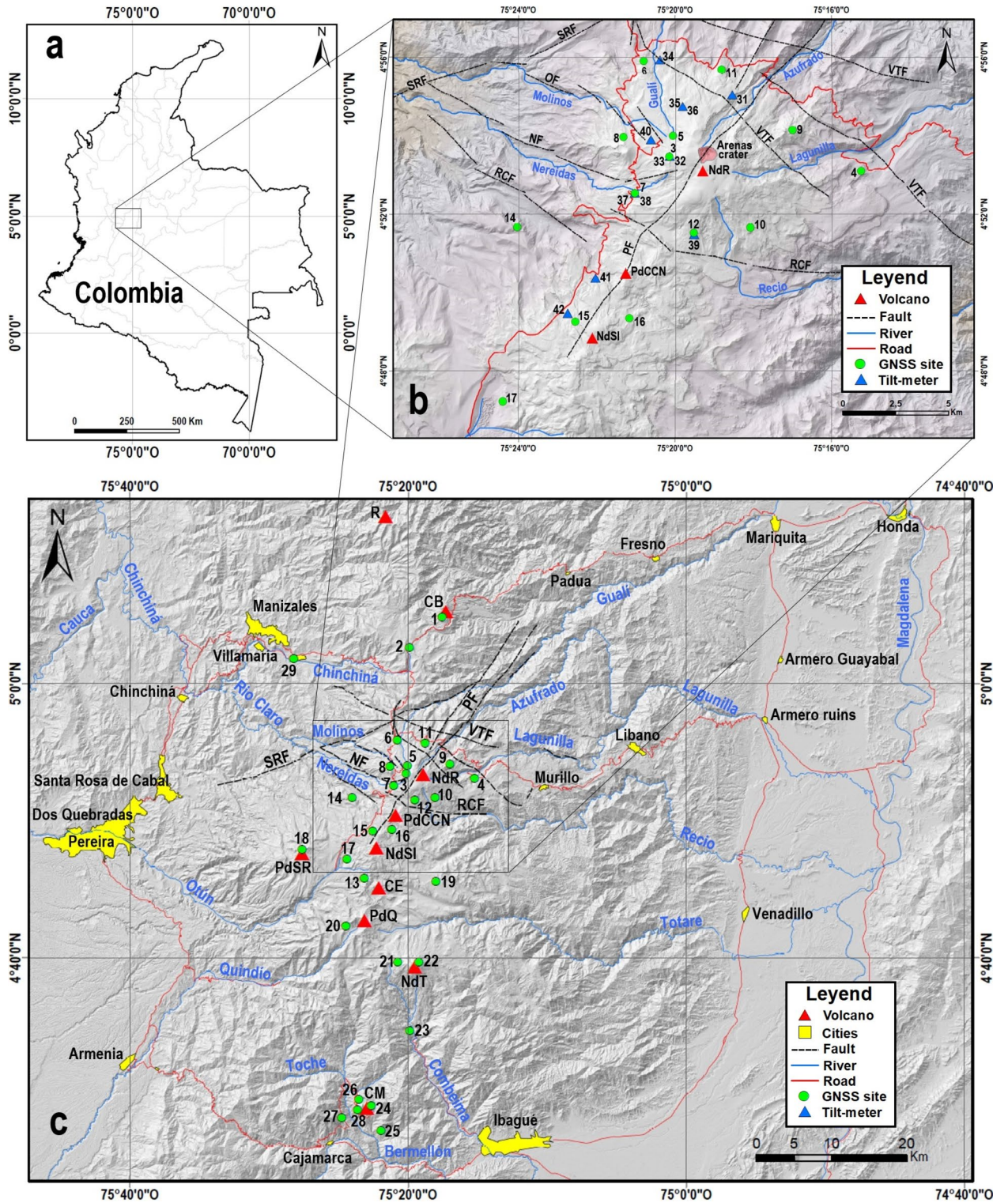
**Fig. 1.** Map of Nevado del Ruiz and its geodetic monitoring networks. (**a**) Map of Colombia with the location of the study area (black square). (**b**) Map of Nevado del Ruiz. Arenas crater: Latitude 4.982° N, longitude −75.319° W, elevation 5321 m a.s.l. (**c**) Map of main volcanoes and faults of the North Volcanic Segment of Colombia. R: Romeral; CB: Cerro Bravo; NdR: Nevado del Ruiz; PdCCN: Paramillo del Cisne—Cerro Negro; NdSI: Nevado de Santa Isabel; PdSR: Paramillo de Santa Rosa; CE: Cerro España; PdQ: Paramillo del Quindío; NdT: Nevado del Tolima; and CM: Cerro Machín. PF: Palestine fault, TVF: Termales-Villamaría fault, OF: Olleta fault, NF: Nereidas fault, RCF: Río Claro fault, and SRF: Santa Rosa fault[1]. Blue triangles: tiltmeters; green circles: GNSS stations (see also Table 1S—Supplementary Material). These maps (**b,c**) were created using ArcGIS software by Esri [www.esri.com], a 90 m DEM from NASA[7], and GIS analysis to produce base maps.

improve the assessment of volcanic hazards, and significantly reduce the volcanic risk. Furthermore, real time information about the state of the volcano has been essential to allow authorities and communities around the volcano to manage the always present volcanic hazards. Nevado del Ruiz has moved from the location of one of the major volcanic disasters in historic times to an example of effective volcanic monitoring that has contributed to better volcanic risk management.

In this article, we present a summary of the recent unrest and dome forming eruption, share information and data about geodetic monitoring of Nevado del Ruiz, model tilt and GNSS data to image the local and regional magma reservoirs, and finally present a conceptual model of the volcanic complex.

## Results
### The geodetic monitoring network

The Volcanological and Seismological Observatory of Manizales—Colombian Geologic Survey (OVSM-SGC) conducted geodetic surveys on Nevado del Ruiz in October 1985, just few days before the eruption, using four dry tiltmeters and two electronic tiltmeters[10]. These tiltmeters were installed 5–7 km northeast of the crater. OVSM-SGC was able to make only eight measurements on the existing network of four dry tiltmeters before the eruption. Unfortunately, the data was very noisy. Due to the limited amount of data collected and its poor quality, no clear deformation pattern indicating an imminent eruption could be identified[11].

After the eruption of November 1985, the Colombian Geological Survey—Volcanological and Seismological Observatory of Manizales (OVSM-SGC) made major efforts to improve the deformation monitoring network, and thanks to the support from the U.S. Geological Survey—Volcano Disaster Assistance Program (VDAP), installed 4 platform electronic tiltmeters, 11 dry tiltmeters, 5 leveling lines, 38 Electronic Distance Measurement (EDM) reflectors, and 8 EDM bases. Unfortunately, the 4 electronic tiltmeters did not operate correctly and were dismantled in 1986. The EDM network was occupied in 1986, but the data did not show a clear deformation pattern[11]. In 2007, a new EDM network was set up and periodically occupied until 2012, when it was abandoned because of the hazards related to the increased activity of the volcano and the constant fall of ash that prevented EDM measurements. The dry tiltmeters and leveling lines were occupied periodically until 2006, and then abandoned because of the lack of any significant data. Two new platform electronic tiltmeters were installed in 2007 and the network was later expanded to 10 sites. Unfortunately, most of the tiltmeters, except for the Refugio (REFU) site, stopped operating at the end of December 2012 (Figs. 1b, 2b). The installation of permanent GNSS stations began in 2011 and today a network of 10 stations continuously monitor deformation at Nevado del Ruiz. A network of 19 additional GNSS stations (Figs. 1c, 2b, 3) and 9 electronic tiltmeters have been installed in the Nevado del Ruiz Volcanic Complex to expand the coverage to the 12 volcanoes of the area and complement the geodetic monitoring of Nevado del Ruiz (Table 1S—Supplementary Material).

Finally, the OVSM-SGC has been routinely using Differential Interferometric Synthetic Aperture Radar (DInSAR) to monitor the deformation at Nevado del Ruiz since 2014, using data available from the ESA Sentinel missions (Fig. 2b).

### Recent unrest and dome forming eruption

Nevado del Ruiz entered a new phase of unrest and eruption in 2010, following an 8-year period of quiescence and 25 years after the tragic eruption of November 1985. Precursory aseismic deflation was observed by tiltmeters between 2010 and early 2012 (Fig. 2b). In September 2010, long period (LP) seismic events (Fig. 2a) and emissions of $SO_2$ (Fig. 2c) increased. The OVSM-SGC increased the alert level from Green (active volcano with low activity) to Yellow (volcano highly active with changes in behavior), but the activity quickly returned to low levels. Tiltmeters and GNSS stations continued to record aseismic deflation between 2010 and early 2012 (Fig. 2b).

In March 2012, there was a significant increase in seismic activity (Fig. 2a), deformation (inflation at a rate of 2–3 cm/yr (Fig. 2b), $SO_2$ release (Fig. 2c) and ash emissions. On March 31st, 2012, the OVSM-SGC increased again the alert level to Orange (probability of eruption in days or weeks). Subsequently, two low energy explosions (VEI 1; Fig. 2a) occurred on May 29th, 2012, and June 30th, 2012. These explosions, with ash columns rising less than 10 km high above the summit, helped clear the volcanic conduit and open the system. The OVSM-SGC then issued a Red alert (eruption is underway). The eruptions generated small lahars, which impacted the proximal area and did not cause any loss of human lives. Proper risk management allowed the OVSM-SGC to successfully manage the crisis[12].

After the 2012 eruptions, the volcano remained in a state of unrest with significant seismicity, inflation, and intermittent emission of water vapor, $SO_2$ and ash. The flux of $SO_2$ reached the extreme values of 35 kton/day in March 2012 and 32 kton/day in September 2015 (Fig. 2c). Short and sporadic 'drumbeat' seismicity started in August 2015, together with inflation, recorded by tiltmeters and GNSS stations (Fig. 2b), and small volcanic explosions, followed by the onset of a dome-forming eruption at the bottom of the main crater (Fig. 2a). The dome continued to grow for several months with fluctuations in the extrusion rate until December 2019, reaching a diameter of approximately 130 m, a maximal height of 60 m, and an approximate volume of $1.7 \times 10^6$ m$^3$ (Fig. 2a)[3].

The volcano has been in a moderate level of activity since the end of 2019, briefly increased in the spring of 2023 by a volcano-tectonic swarm (Fig. 2a), minor explosions, ash emissions, and gas release (Fig. 2c).

### GNSS time series

We divided the GNSS time series into six stages based on changes in vertical displacement and deformation velocities (Figs. 3, 1S, and Table 2S—Supplementary Material). To define these stages and their corresponding deformation velocities, we followed a two-steps approach. First, we modeled the GNSS deformation velocity by fitting a logarithmic regression to the displacements. This approach effectively captured the rapid decay in the
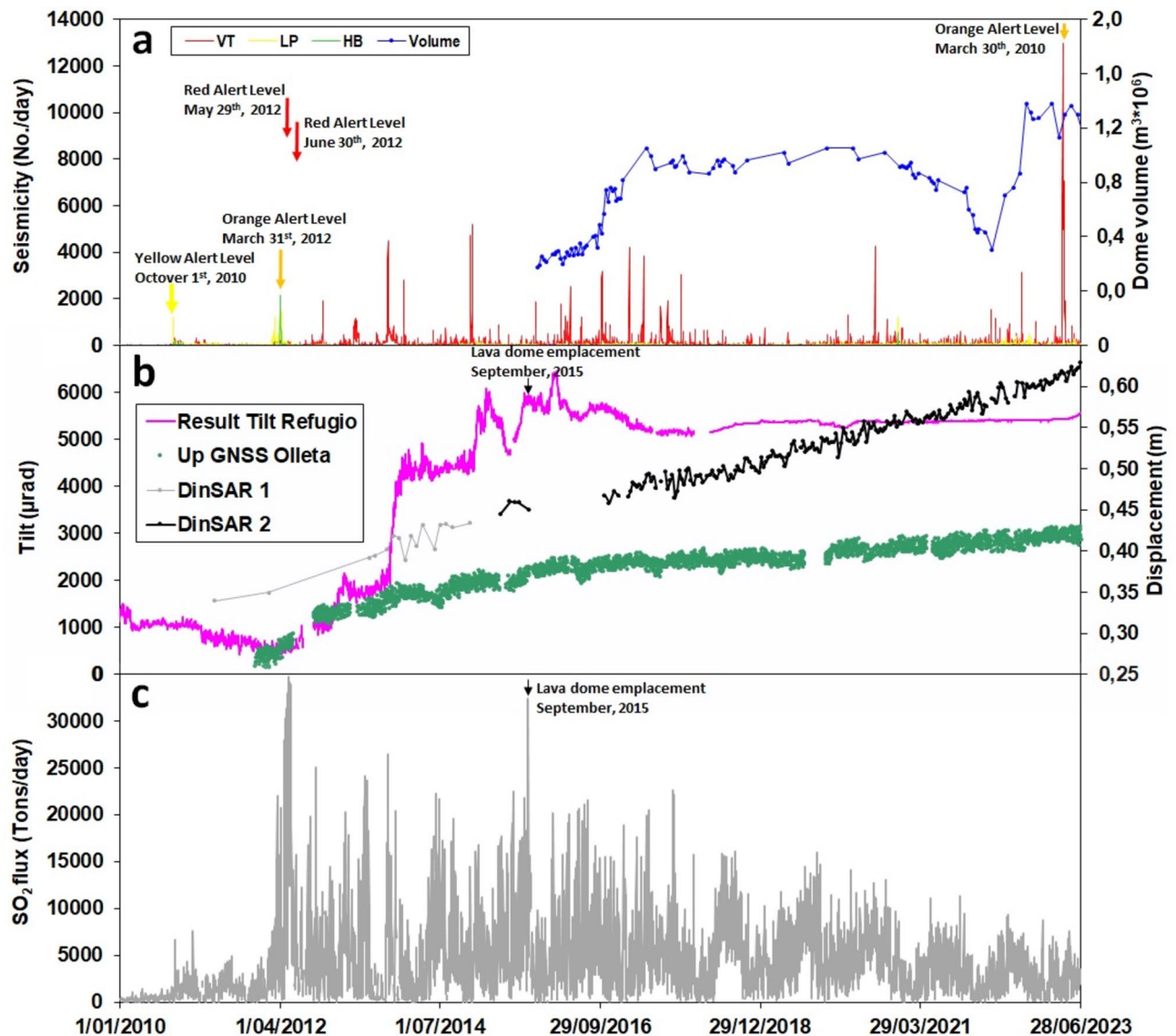
**Fig. 2.** Nevado del Ruiz multiparametric plots of seismic, geodetic, geochemical, and lava dome-forming eruption data from 2010 to 2023. (**a**) **Seismicity**. Red line: volcano-tectonic (VT) events. Yellow line: long period (LP) events. Green line: hybrid (HB) events. Blue line with dots: lava dome volume. Yellow arrow: yellow alert (volcano very active). Orange arrow: orange alert (probability of eruption). Red arrow: red alert (eruption). (**b**) **Tilt**. Magenta line: resulting tilt component from the Refugio (REFU) tiltmeter. **GNSS**. Green dots: vertical displacement at the Olleta (OLLE) GNSS site (see Fig. 1b for locations). **DinSAR**. Gray line with dots: line-of-sight (LOS) obtained from ascending RADARSAT-2 observations (DInSAR 1) estimated at the OLLE GNNS site[8]. Black line with dots: LOS obtained from ascending SENTINEL-1 observations estimated at the OLLE GNNS site (DInSAR 2). (**c**) **Gas discharge**. Grey line: $SO_2$ flux in tons/day.

acceleration of the deformation velocity. Our findings indicate that the deformation during stage 2 was more accelerated compared to stages 3 and 5 (see Fig. 2S in Supplementary Material). Then, we approximated the displacements trend at each stage using a straight line. This allowed us to estimate the slope of each line and the deformation velocities for each stage (see Fig. 2S in Supplementary Material).

The volcano surface was subsiding aseismically until February 2012. The inflation of the volcano edifice started in March 2012 and continued intermittently until spring of 2023 with periods of deformation interspersed with periods of quiescence. We estimated GNSS deformation velocities for stage 1 (2010 installation year of the first GNSS station—to February 2012), stage 2 (March to November 2012), stage 3 (December 2012 to November 2017), and stage 5 (June 2019 to March 2023). Stage 4 (December 2017 to June 2019) and stage 6 (April 2023 to present) did not have a significant deformation even when the volcano was highly active.
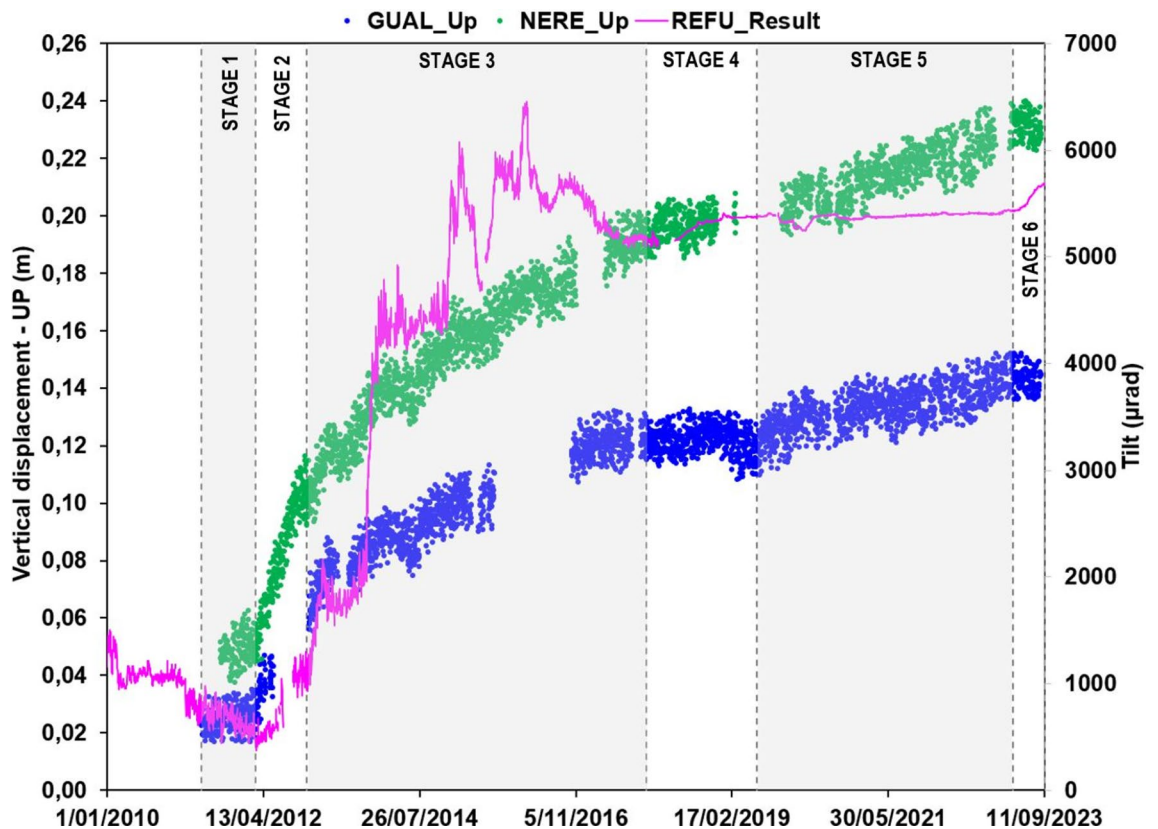
**Fig. 3.** Vertical displacement time series of the GNSS sites Gualí (GUAL_Up) and Nereidas (NERE_Up) versus the tilt resulting component at the Refugio tiltmeter (REFU_Result) from 2010 to 2023. Time series for all GNSS sites of Nevado del Ruiz are available in Fig. 1S—Supplementary Material.

### Tilt time series

We divided the tilt time series from REFU into various stages according to the tilt rate changes (Figs. 3, 3S, and Table 3S—Supplementary Material). Tilt time series show a trend like that recorded by the GNSS stations with the volcanic edifice subsiding aseismically until February 2012. The uplift of the volcano surface began in March 2012 and continued until February 2016. A minor subsidence was recorded from February 2016 to the end of 2017, when the tiltmeter stabilized and stopped recording any significant deformation. We estimated the tilt only for stages 1 and 2, since tiltmeters began to operate erratically after stage 2. During tilt stages 2 and 3, the REFU tiltmeter recorded several uplift episodes triggered by the occurrence of VT events, followed by periods of either rapid subsidence or quiescence (Fig. 3S—Supplementary Material). See also details of stages definition in chapter "Stage Definition" in Supplementary Material.

### Modeling

Results from the non-linear inversion of tilt and GNSS data from Nevado del Ruiz are summarized in Table 1 for each tilt and GNSS stages (see also Tables 4S, 5S and 6S—Supplementary Material for more details).

The subsidence observed in the tilt time series (Fig. 4) during Stage-1 was caused by the depressurization of a shallow source located beneath the crater of Nevado del Ruiz at a depth of $4.6 \pm 1.2$ km, with a volume change of $-0.009 \pm 0.007$ km$^3$.

In Stage-2, early 2012, the nonlinear uplift detected in the tilt time series (Fig. 4) can be attributed to a volume increase of $0.015 \pm 0.001$ km$^3$ from a shallow source $2.5 \pm 1$ km beneath the crater of Nevado del Ruiz. The uplift of approximately 6.5 cm observed in the GNSS time series (Fig. 5) is linked to a volume increase of $0.069 \pm 0.019$ km$^3$ from a deeper source, located $8.4 \pm 0.6$ km southwest of Nevado del Ruiz, at a depth of $15.2 \pm 0.9$ km beneath Nevado de Santa Isabel.

Stage-3 saw a total uplift of about 8.5 cm in the GNSS time series (Fig. 5), resulting from a volume increase of $0.10 \pm 0.02$ km$^3$ from a deep source located $11.1 \pm 1.2$ km southwest of Nevado del Ruiz, at a depth of $13.8 \pm 1.2$ km beneath Nevado de Santa Isabel.

Finally, during Stage-5, the uplift observed in the GNSS time series (Fig. 5) was driven by a volume increase of $0.017 \pm 0.008$ km$^3$ always from a deep source at a depth of $15 \pm 2$ km. beneath Nevado de Santa Isabel, $10.3 \pm 0.8$ km southwest of Nevado del Ruiz.

Following Stage-5, the GNSS network recorded minimal or no deformation in Stage-6 (Fig. 3 and Table 1).

| | Observation | | | Modelling | | | Interpretation |
|---|---|---|---|---|---|---|---|
| Stage | Technique | Surface change | Deformation type | Model | Location | Source | Reservoir |
| 1 | Tiltmeter GNSS | Subsidence | Deflation | Depressurization | Nevado del Ruiz | Shallow | Local |
| 2 | Tiltmeter GNSS | Uplift | Inflation | Pressurization | Nevado del Ruiz Nevado de Santa Isabel | Shallow Deep | Local Regional |
| 3 | GNSS | Uplift | Inflation | Pressurization | Nevado de Santa Isabel | Deep | Regional |
| 4 | GNSS | No changes | No deformation | | | | |
| 5 | GNSS | Uplift | Inflation | Pressurization | Nevado de Santa Isabel | Deep | Regional |
| 6 | GNSS | No changes | No deformation | | | | |

**Table 1.** Volcano surface deformation (uplift/subsidence/no deformation) recorded by tiltmeters and GNSS stations for the six deformation stages of Nevado del Ruiz, and the results from modelling. The deformation type describes the phenomena process causing deformation (inflation/deflation). The modelling shows the type of shallow/deep source causing depressurization/pressurization of the volcano, and the relation with the local, shallow magmatic reservoir located beneath Nevado del Ruiz, and the deep, regional magmatic reservoir located beneath Nevado de Santa Isabel.
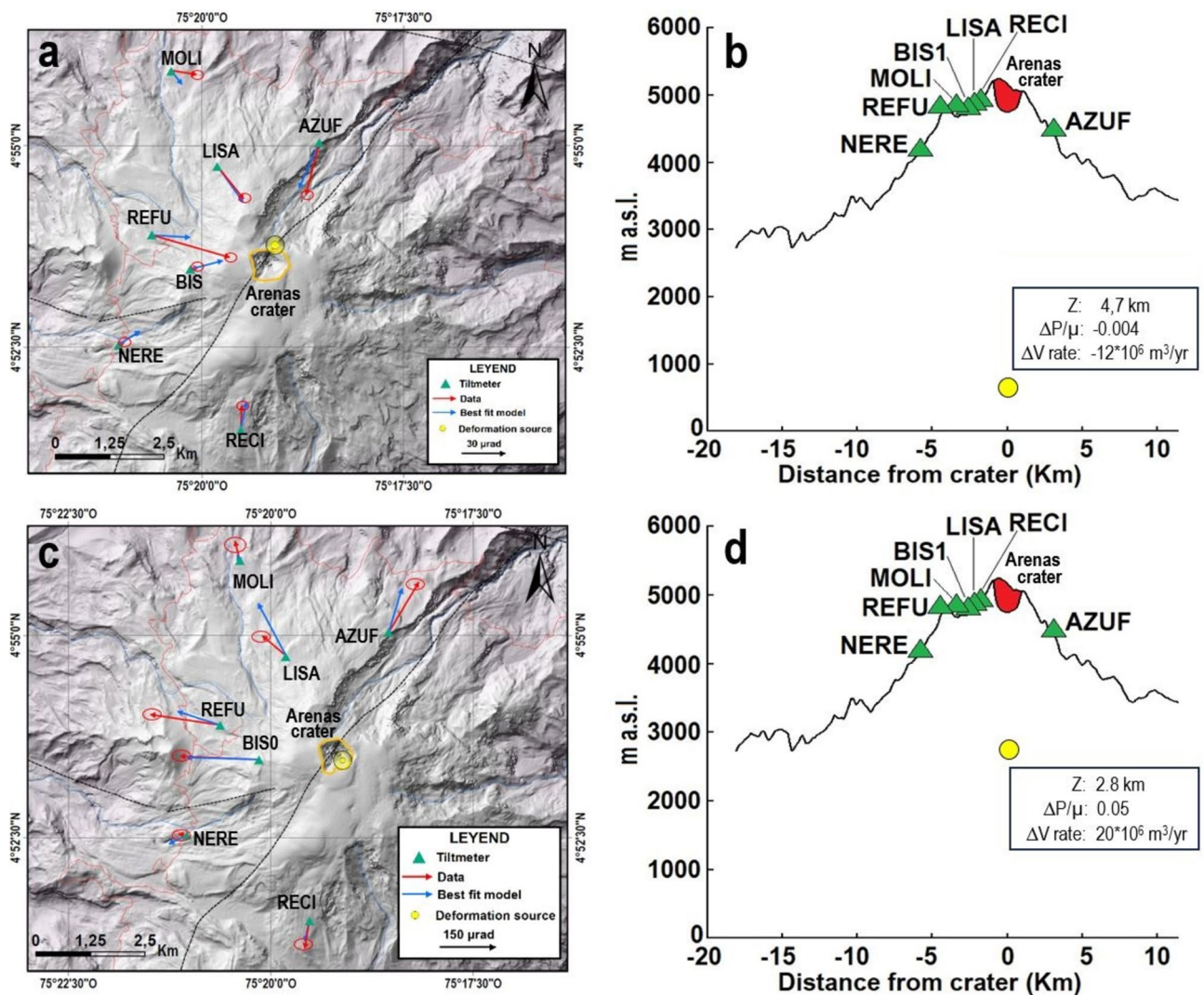


**Fig. 4.** Vector plot maps and profiles of tilt deformation for Nevado del Ruiz. (**a,b**) Stage-1; (**c,d**) Stage-2. Red arrows: observed tilt; blue arrows: predicted tilt; red ellipses: data errors; yellow circle: position of the spherical source employed to model the data. The background is the NASA 90 m DEM[7]. The results are consistent with a source located near the main crater of Nevado del Ruiz. Source depth and rate of volume change are in the boxes in panel (**b**) and (**d**). These maps (**a,c**) were created using ArcGIS software by Esri [www.esri.com], a 90 m DEM from NASA[7], and GIS analysis to produce base maps.
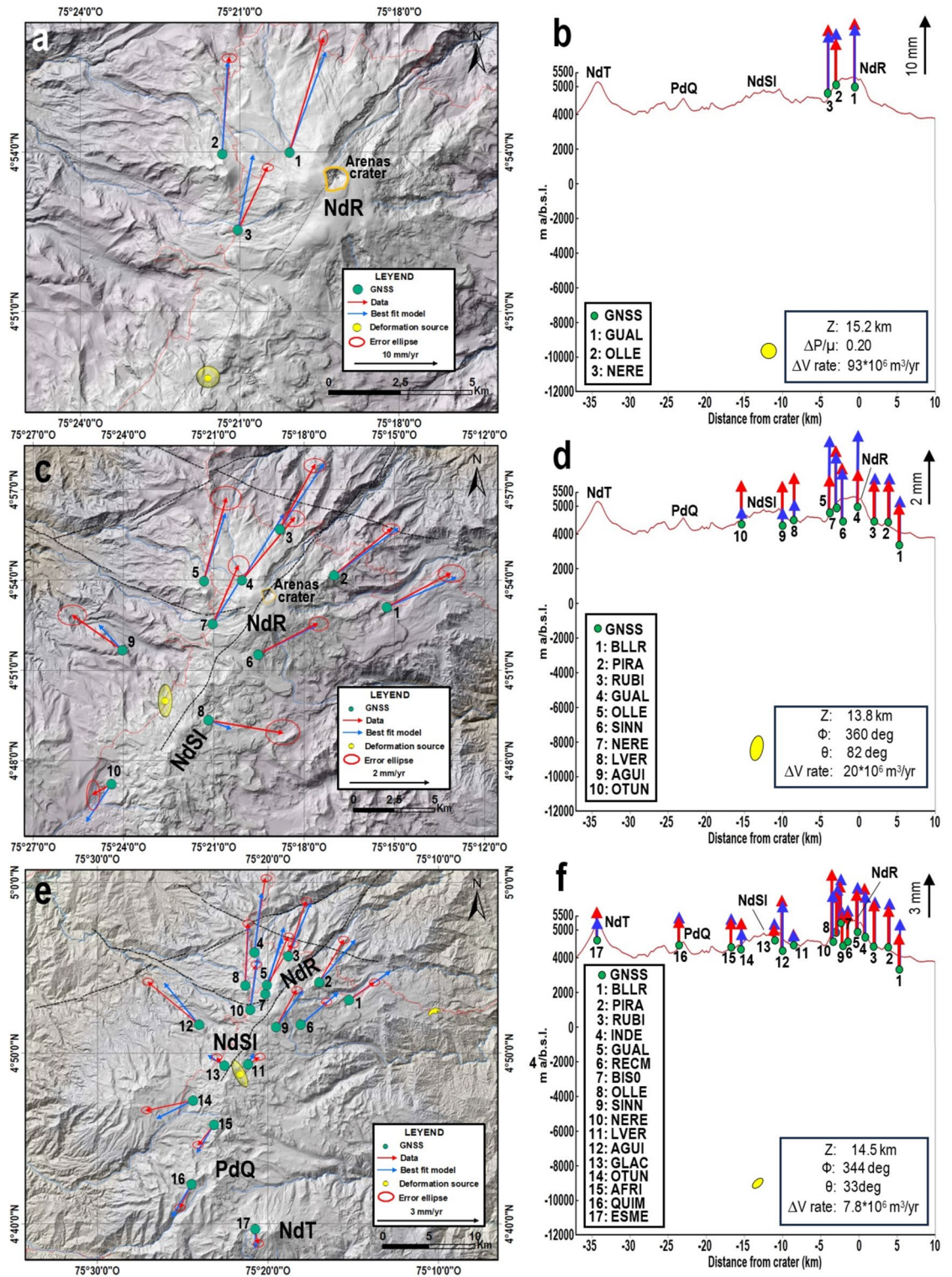
**Fig. 5.** Vector plot and profiles of horizontal GNSS deformation for Nevado del Ruiz. (**a,b**) Stage-2; (**c,d**) Stage-3; (**e,f**) Stage-5. Red arrows: observed tilt; blue arrows: predicted tilt; red ellipses: data errors; yellow circle: position of the spherical source for modeling. The background is the NASA 90 m DEM[7]. The best fit is achieved with a spherical model for Stage-2, and a spheroidal model for Stages-3 and Stage-5. Source depth and rate of volume change are provided in the boxes in panel (**b**) (**d**) and (**f**). Only three GNSS sites were available during Stage-2, which affected the results due to gaps in the GNSS monitoring network. During Stages-3 and Stage-5, the number of monitoring sites had increased to 11 and 17 GNSS stations, respectively. Therefore, we expect the modeling results to be more robust for Stage-3 and Stage-5 compared to Stage-2. These maps (**a,c,e**) were created using ArcGIS software by Esri [www.esri.com], a 90 m DEM from NASA[7], and GIS analysis to produce base maps.

## Summary and conclusions

Data from Nevado del Ruiz demonstrates that tiltmeters are extremely sensitive to detecting small, localized deformations that may go unnoticed by GNSS. According to our analysis, the tiltmeters monitoring Nevado del Ruiz are sensitive to changes in pressure in a shallow, local reservoir, within the volcanic edifice, which is feeding the ash emissions, gas release, small explosions, and the dome forming eruption. On the other hand, the deformation recorded by the GNSS network is the response of the volcanic surface to the recharge of a deep, regional reservoir located beneath Nevado de Santa Isabel, about 9 km southwest of Nevado del Ruiz.

Although we do not have a clear explanation for the reactivation of the shallow magmatic system of Nevado del Ruiz by the deep magmatic system beneath Nevado de Santa Isabel yet, this study confirms that the existence of a laterally extended magmatic system, defined as the location of deformation sources that are ≥ 5 km away from the nearest active volcanic vent, is a common occurrence in the Andean volcanoes[13,14].

The subsidence of the volcano surface recorded by tiltmeters (since 2008) and GNSS stations (since 2011) until February 2012 is associated to a long aseismic deflation of the volcanic edifice. Modelling of tilt data points to the potential depressurization of a shallow reservoir, located 2.7 – 4.6 km below the main crater of Nevado del Ruiz (see Tables 4S, and 5S—Supplementary Material). This shallow reservoir is considered the local reservoir of the volcano and for the past 13 years has been the source for gas release, ash emissions, minor explosions, and the dome forming eruption.

The interpretation of the tilt modelling may be unclear because the two inferred sources, T1 and T2, do not overlap within 1 standard deviation, though they do overlap within 2 standard deviations (Table 4S). This ambiguity can be resolved by comparing the depth of these sources with the model for the activity of Nevado del Ruiz proposed by[15]. This model, based on a seismic tomography study using over 1,500 high-quality regional and local events, identified zones with low P wave velocity (low-VP) and low S wave velocity (low-VS). One low-VS zone is located at depths of 2–4 km beneath the volcano vent, aligning with our source T2 (Table S4 and Fig. 6). The second low-VP and low-VS zone is found at depths of 5–10 km beneath the volcano vent. Our deformation source T1 matches the roof of this zone (Table S4 and Fig. 6).

The perturbed, non-linear deformation recorded by REFU tiltmeter is caused by the high sensitivity of this instrument. The rapid alternance of surface uplift/subsidence episodes, triggered by VT events, reflects minor episodes of inflation/deflation of the volcano caused by the changes in the pressurization of the shallow, local reservoir. This tiltmeter did not record any significant deformation after February 2016, a sign that the shallow magma reservoir has been in equilibrium with the external environment because of the open conduit feeding the dome-forming eruption.
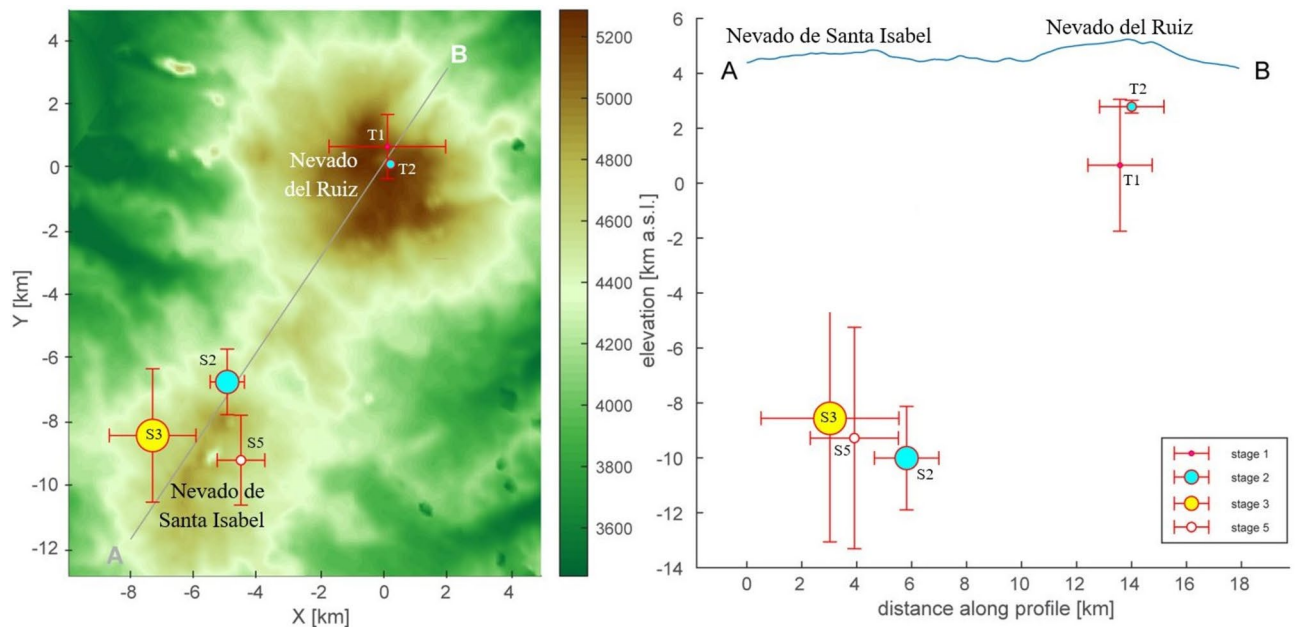


**Fig. 6.** Map (left) and SW-NE (A-B) profile (right) from Nevado de Santa Isabel (SW corner) to Nevado del Ruiz (NE corner) with the location of the deformation sources for each stage. Error bars are one sigma (68% confidence level); vertical error bars for T2 are of the same magnitude of the marker. The size of the symbol is proportional to the volume of the intrusion (see Tables 4S, 5S, and 6S—Supplementary Material). The shallow magma reservoir is located 2.7–4.6 km beneath the vent of Nevado del Ruiz, and it is considered the local reservoir. The regional, deep magma reservoir is located approximately 9 km SW from Nevado del Ruiz, at a depth of 11–16 km beneath Nevado de Santa Isabel. DEM model from the USGS Earth Explorer web site (https://earthexplorer.usgs.gov/). Tilt analysis for stage-1 (T1), and stage-2 (T2); GNSS analysis for stage-2 (S2), stage-3 (S3), and stage-5 (S5). This map was created using MATLAB software [www.mathworks.com], and a 90 m DEM from NASA[7].

Modelling of GNSS deformation velocities infer the recharge of a deep magmatic reservoir below Nevado de Santa Isabel from three different magma batches (see Figs. 6, 7, and Table 6S—Supplementary Material) in a zone without significant seismicity, located at the base of what is probably a regional reservoir feeding the Nevado del Ruiz Volcanic Complex. Although geodetic data do not indicate a direct connection between the two magmatic systems, the deformation zone lies directly beneath the Palestina Fault (Fig. 7) and is linked to a compressive regional stress zone[8]. The Palestina Fault has been the site of significant volcano-tectonic seismic activity between Nevado de Santa Isabel and Nevado del Ruiz (Fig. 7). We interpret that magma or magmatic fluids from the deep magmatic system beneath Nevado de Santa Isabel are moving toward Nevado del Ruiz through complex pathways identified by the hypocenters of this seismic activity.

The locations and depths of the deformation sources beneath Nevado de Santa Isabel inferred from GNSS compare well against the results from the InSAR data inversion made by[8], although the volume change (0.08 km$^3$) calculated is smaller since the analysis was from 2012 to 2014 only.

Approximately 0.185–0.195 km$^3$ of magma/fluids have been intruding between 2012 and 2023 in the deep regional reservoir. It is not clear how the pressurization of this deep reservoir reactivated Nevado del Ruiz without
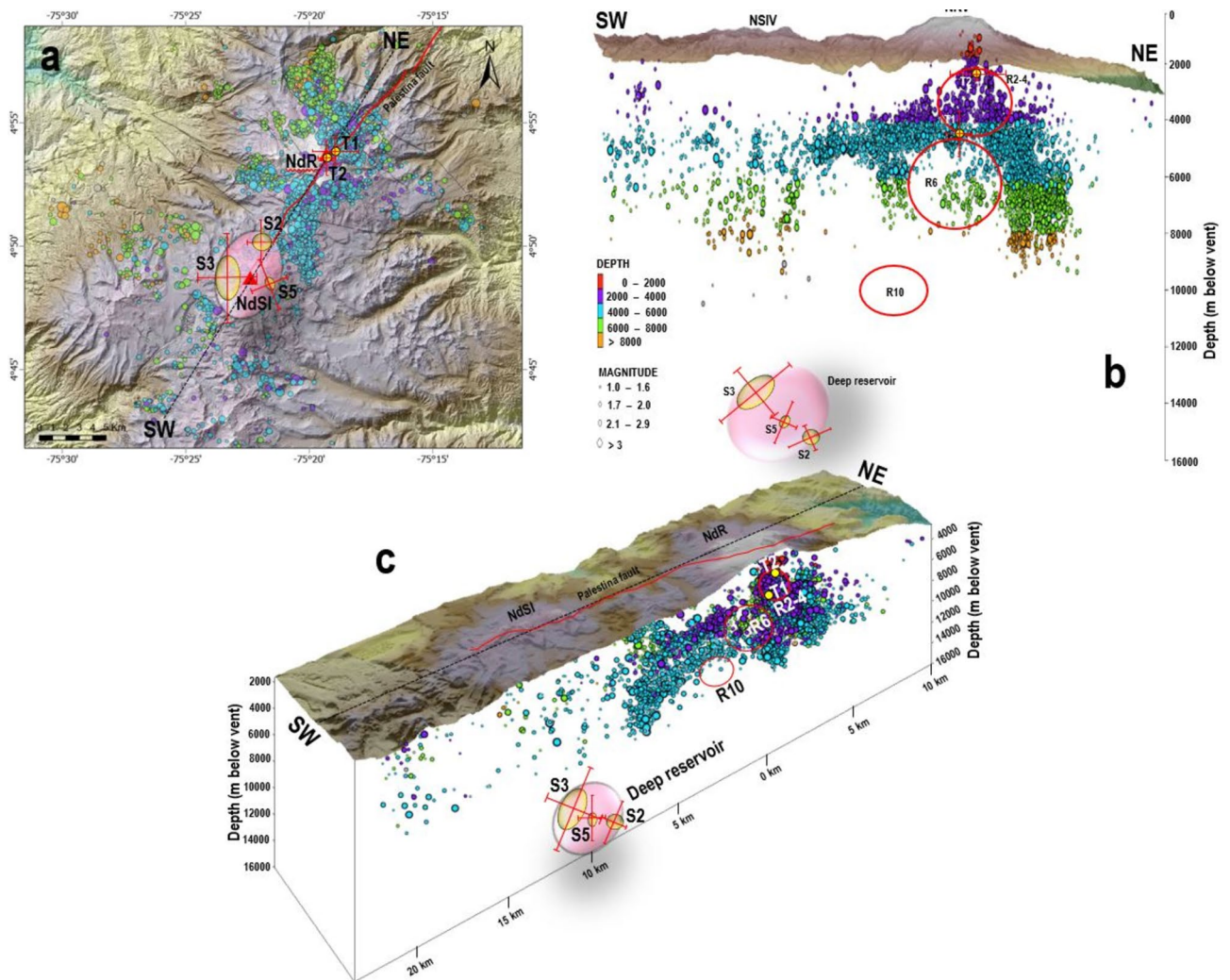


**Fig. 7.** Location of volcano-tectonic seismicity and deformation sources from 2010 to 2023 relative to the reference elevation of 5231 m (height of Nevado del Ruiz). (**a**) Map view. (**b**) SW-NE cross-section (black dashed line on the map view) through Nevado de Santa Isabel and Nevado del Ruiz. (**c**) 3D projection of the seismicity location and deformation sources. Seismicity depth and its local magnitude are represented using color and circle size. Yellow circles and ellipses represent the modeling deformation source locations and depths resulted from the tilt analysis for stage-1 (T1), and stage-2 (T2); and GNSS analysis for stage-2 (S2), stage-3 (S3), and stage-5 (S5). The local, shallow deformation source is located 2.7–4.6 km depth beneath the Nevado del Ruiz crater, it is considered the local reservoir, and should be part of the shallow magma chamber imaged by seismic tomography[15]. R6: intermediate magma chamber; R10: main magma chamber. The regional, deep reservoir (pink ellipse) is located approximately 9 km SW from Nevado del Ruiz, 11–16 km beneath Nevado de Santa Isabel, and should identified as part of the tripartite magma chamber imaged by seismic tomography[15]. These maps were created using ArcGIS software by Esri [www.esri.com], a 90 m DEM from NASA[7], and GIS analysis to produce base maps.

any change in the background level of activity of Nevado de Santa Isabel. Analysis of the products released during the eruptive episodes of Nevado del Ruiz suggests that magma from this deep magma reservoir has not reached the shallow reservoir of Nevado del Ruiz yet.

The uplift of the volcano surface recorded by GNSS stations until spring of 2023 is associated to the slow, but continuous recharge of a regional reservoir. Modelling suggests the potential pressurization of a deep reservoir located 8.2–9.8 km southwest of Nevado del Ruiz, and 11–16 km beneath Nevado de Santa Isabel (Figs. 6, 7).

The GNSS time series presents three main deformation periods, stages 2, 3 and 5, interspersed with 2 periods of quiescence. Stage 2 has the largest deformation velocity, the high surface acceleration estimated during this stage is due to the reactivation of the volcano, and the two eruptions on May 29th and June 30th, 2012. Stages 3 and 5 have a slower, constant deformation acceleration, in agreement with the reduced but continuous activity of the volcano (Figs. 2 and 1S).

The deep reservoir is part of the tripartite magma chamber imaged by seismic tomography[15]. The interpretation of the seismic tomography is that a main reservoir of magma at a depth of approximately 10 km (R10 in Fig. 7) feeds an intermediate chamber at a depth of ~ 6 km (R6 in Fig. 7). The intermediate reservoir should be connected to a shallow magma chamber 2–4 km deep (R2-4 in Fig. 7) where most of the seismicity is occurring, and the source of the 2015 dome forming eruption.

Repeated tomographic inversions[16] found a high $V_P/V_S$ anomaly beneath Nevado del Ruiz, attributed to the presence of volatiles-rich magma in a shallow reservoir. The upper boundary of this anomaly, interpreted as the roof of the reservoir, lies at ~ 2 km depth (R2-4 in Fig. 7). This result is consistent with the shallow reservoir inferred by the modelling of tilt data (Fig. 4, and Table 4S—Supplementary Material).

The volcano has now been continuously active since 2012 with seismicity, deformation, ash emissions, low energy explosions (VEI = 1), gas release, and a dome forming eruption. The integration of geodetic monitoring with seismic, geochemical, and geological observations has enhanced our understanding of the behavior of the volcano, improving the assessment of volcanic hazards, and significantly reduced the volcanic risk. Monitoring data, collected in real time, are analyzed, and interpreted daily. The main findings and alerts are routinely reported to the public through the web page and social media by the OVSM-SGC (https://www2.sgc.gov.co/sgc/volcanes/VolcanNevadoRuiz/Paginas/generalidades-volcan-nevado-ruiz.aspx). Thanks to these efforts and open communication channels between the volcano observatory, local authorities, and the public, Nevado del Ruiz has transitioned from being the site of one of the most significant volcanic tragedies in history to becoming a model of successful volcanic risk management.

## Methods

### Tiltmeters

Platform mount tiltmeters are electronic instruments design for high precision/sensitivity tilt measurements (0.1–1 μrad with virtually zero long-term drift), analog and digital output and low power consumption. They have a horizontal triangular platform made of aluminum or stainless steel, on which two electrolytic sensors are attached (parallel to the sides of the triangle, orthogonal to each other, and north/east magnetic oriented), a temperature sensor, an electronic card, and includes two switchable gains (low and high) and two low-pass filter settings. Each tiltmeter has an aluminum or stainless-steel cover that is attached to the platform to protect the sensors and the electronic board. The platform is provided with 3 built-in invar leveling legs for easy installation on any horizontal surface. Tilt changes in the surface are detected by resistance changes as response to the rotation of the electrolytic sensor, convert to voltage changes and into tilt angles in the north and east components that can be combined to obtain a resulting tilt component. Simultaneously, the voltage reading of the temperature sensor is converted to degrees Celsius. This information can be transmitted via radio with a specific sampling rate to the observatory, where the signal is received by a computer.

### Global, regional, and local GNSS reference frames

To stabilize the GNSS solutions, we defined a global and a regional reference frame by imposing generalized constraints on the solutions. This involved estimating the translation and rotation parameters of the frame (Helmert parameters) and minimizing the adjustments of coordinates to filter the long-term (secular) tectonic deformation. This approach allowed us to emphasize the much more rapid volcanic deformation[17]. Additionally, we established a local reference frame to impose constraints on the solution, minimizing the coordinate adjustments to just two GNSS stations. This method avoids the need for translation and rotation during stabilization, allowing us to directly extract the volcanic deformation[17]. The global reference frame is defined by 19 GNSS stations of the International GNSS Service network (IGS, https://igs.org/network/) located in the stable N, NE, and E cratons of the South America tectonic plate. The regional reference frame is defined by 22 GNSS stations of the Regional Geodetic Network of Colombia, https://geored.sgc.gov.co[18], that define the slow tectonic deformation of the North Andes Block (located in the NW corner of the South America plate). The local reference frame is fixed to 2 very stable GNSS stations in Cerro Machin with no deformation, located 45 km southern of Nevado del Ruiz. The stabilization results of the regional and local frames are the same.

### GNSS time series

Daily GNSS solutions were processed with GAMIT/GLOBK, version 10.71 (http://geoweb.mit.edu/gg;[17]). We approached the GNSS data processing following the three-steps method described in[19], summarized in: phase data analysis, combination of solution, and position time-series analysis. In the first step of the data processing, we estimated daily loosely constrained solutions and covariance of station coordinates, orbital and Earth orientation parameters, atmospheric delays, and ambiguities, applying loose a priori constraints to all parameters. The daily loose-constrained solutions and their covariance were used in the second step to compute time series and

deformation velocities. We determined the weights for each set of quasi-observations by averaging the increments in chi-square per degree of freedom from forward and backward filtering of the data. In the third step, we imposed a general constraint in position and velocity to define a uniform reference frame. This stabilization process is necessary to obtain time series of station coordinates, which can then be plotted and examined to remove possible outliers. The initial input for GAMIT/GLOBK was the GNSS carrier phase and other observables, sampled at 30 s intervals with a 10° elevation mask. The daily position solutions were computed using precise ephemerides provided by the International GNSS Service (https://igs.org). The results of this analysis are time series of the GNSS stations East, North and Up coordinates, and their deformation velocities (Fig. 3). Uncertainties of the deformation velocities are estimated using the real-sigma algorithm implemented in GLOBK[17].

### Tilt time series

Tiltmeters monitoring Nevado del Ruiz are installed in dedicated vaults beneath the surface in stable outcrops, fastened to a polished rock surface. This setup uses a high-density styrofoam sheet to isolate the vault, significantly reducing the temperature oscillations (around 1 to 3 °C) and the environmental noise. Postprocessing can eliminate the effects from the linear drift of the instrument and possible cyclic fluctuation associated with the external temperature and earth tides. Unfortunately, most of the tiltmeters, apart from the site Refugio (REFU), stopped operating at the end of December 2012.

*Modeling*

We modeled the tilt and GNSS deformation using the U.S. Geological Survey software dMODELS[20]. dMODELS implements analytical solutions of several source geometries, commonly employed in volcano geodesy. Analytical solutions approximate the actual deformation sources with pressurized cavities in a homogenous, elastic half-space. We applied a topography correction for the spherical source only[21]. It is worth noting that these cavities are not material sources. They are only convenient mathematical devices mimicking the stress and potential field changes generated by the actual sources of unrest[22]. Although analytical models are based on several simplifications (e.g., the assumption that the crust is a homogenous, isotropic, elastic medium) that make the set of differential equations describing the problem tractable, they can consider a vast array of source geometries and the influence of topography[21,23–26]. The careful use of analytical models, together with high quality data sets, can yield valuable insights into the nature of the deformation source.

We reduced the inherent non-uniqueness of non-linear inversions (e.g.,[22]) by adopting a redundant modeling strategy: (a) we increased the number of random searches in the non-linear inversions from an initial 64 random searches to 512; and (b) we inverted the data sets using different sources. Our preferred solutions are stable solutions (independent the number of random grid searches), in good agreement with the known geology and distribution of earthquakes.

### Data availability

GNSS and tilt site locations are available in Table 1S—Supplementary Material. GNSS deformation velocities and tilt deformation data are available in Tables 2S, and 3S—Supplementary Material. Additional information about data employed in this paper, and the results of GNSS and tilt data modelling are available in the Supplementary Material. Modeling software, complete data set and inversion results are available online at https://doi.org/10.5281/zenodo.12194034 [27]. Maps throughout this manuscript (Figs. 1, 4, 5, 7) were created using ArcGIS® software by Esri [ArcGIS® and ArcMap™ are the intellectual property of Esri and are used herein under license. Copyright © Esri. All rights reserved. For more information about Esri® software, please visit www.esri.com], a 90 m DEM from NASA[7], and GIS analysis to produce base maps. Maps of Fig. 6 of this manuscript were created using MATLAB® software version R2023b by Mathworks Inc. [MATLAB® is the intellectual property of Mathworks Inc. and is used herein under license. Copyright © Mathworks Inc. All rights reserved. For more information about MATLAB® software, please visit www.mathworks.com], and a 90 m DEM from NASA[7]. You can contact Maurizio Battaglia at mbattaglia@usgs.gov for the latest version of dMODELS, and Milton Ordonez at mordonez@sgc.gov.co for inquiries regarding GNSS and tilt data.

### References

1. Ceballos-Hernández, J. L., Martínez-Tabares, L. M., Valencia-Ramírez, L. G., Pulgarín-Alzate, B. A., Correa-Tamayo, A. M., & Narváez-Marulanda, B. L. Geological evolution of the NR Volcanic Complex. In *The Geology of Colombia, Volume 4 Quaternary. Servicio Geológico Colombiano, Publicaciones Geológicas Especiales*, Vol. 38 (eds Gómez, J. & Pinilla, A. O.) 267–296 (2020).https://doi.org/10.32685/pub.esp.38.2019.07.
2. González-García, J., Hauser, J., Annetts, D., Franco, J., Vallejo, E., & Regenauer-Lieb, K. Nevado del Ruiz Volcano (Colombia): A 3D model combining geological and geophysical information. In *Proceedings World Geothermal Congress 2015, Melbourne, Australia, 19–25 April 2015* 1–11 (2015).
3. Ordoñez, M., Laverde, C. & Battaglia, M. The new lava dome growth of Nevado del Ruiz (2015–2021). *J. Volcanol. Geotherm. Res.* **430**, 107626. https://doi.org/10.1016/j.jvolgeores.2022.107626 (2022).
4. Pierson, T. C., Janda, R. J., Thouret, J. C. & Borrero, C. A. Perturbation and melting of snow and ice by the 13 November 1985 eruption of Nevado del Ruiz, Colombia, and consequent mobilization, flow, and deposition of lahars. *J. Volcanol. Geotherm. Res.* **41**(1–4), 17–66. https://doi.org/10.1016/0377-0273(90)90082-Q (1990).
5. Londoño, J. M. & Galvis, B. Seismic data, photographic images and physical modeling of volcanic plumes as a tool for monitoring the activity of Nevado del Ruiz Volcano. *Colombia. Front Earth Sci* **6**(162), 1–20. https://doi.org/10.3389/feart.2018.00162 (2018).

6. Méndez, R. & Tadeo, H. La erupción del Volcán Nevado del Ruiz El Primero de Septiembre de 1989. Datos geológicos y modelo de la erupción. Bol. Geol., VOL. 35 No. 2–3, INGEOMINAS. https://revistas.sgc.gov.co/index.php/boletingeo/article/view/292/260 (1995).

7. Jarvis, A., Guevara, E., Reuter, H. I. and Nelson, A. D. (2008). Hole-filled SRTM for the globe: version 4 data grid available from the CGIAR-CSI SRTM 90m Database. CGIAR Consortium for Spatial Information. Available online at http://srtm.csi.cgiar.org, and https://cgiarcsi.community/data/srtm-30m-digital-elevation-database-v4-1.

8. Lundgren, P., Samsonov, S. V., López Velez, C. M. & Ordoñez, M. I. Deep source model for Nevado del Ruiz Volcano, Colombia, constrained by interferometric synthetic aperture radar observations. Geophys. Res. Lett. 42, 4816–4823. https://doi.org/10.1002/2015GL063858 (2015).

9. Castaño, L. M. et al. Continuous monitoring of the 2015–2018 Nevado del Ruiz activity, Colombia, using satellite infrared images and local infrasound records. Earth Planets Space 72, 81. https://doi.org/10.1186/s40623-020-01197-z (2020).

10. Ewert, J. & Swanson. D. Monitoring volcanoes: Techniques and strategies used by the staff of the Cascades Volcano Observatory, 1980–90. USGS Numbered Series, Bulletin 1966. https://doi.org/10.3133/b1966_1992(1992).

11. Banks, N., Carvajal, C., Mora, H. & Tryggvason, E. Deformation monitoring at Nevado del Ruiz, Colombia: October 1985–March 1988. J. Volcanol. Geotherm. Res. 41, 269–295. https://doi.org/10.1016/0377-0273(90)90092-T (1990).

12. Servicio Geológico Colombiano. Informe de actividad volcánica Segmento Norte de Colombia. Complejo Volcánico (Cerro Bravo-Cerro Machín) 2012. Internal report, 96 pp., in Spanish. https://www2.sgc.gov.co/Publicaciones/Informes%20tcnicos/Informe%20t%C3%A9cnico%20anual%20de%202012.pdf (2012).

13. Ebmeier, S. K. et al. Synthesis of global satellite observations of magmatic and volcanic deformation: Implications for volcano monitoring & the lateral extent of magmatic domains. J. Appl. Volcanol. 7, 2. https://doi.org/10.1186/s13617-018-0071-3 (2018).

14. Lerner, A. H. et al. The prevalence and significance of offset magma reservoirs at arc volcanoes. Geophys. Res. Lett. 47, e2020GL087856. https://doi.org/10.1029/2020GL087856 (2020).

15. Londoño, J. M. & Sudo, Y. Velocity structure and a seismic model for Nevado del Ruiz Volcano (Colombia). J. Volcanol. Geotherm. Res. 119(1–4), 61–87. https://doi.org/10.1016/S0377-0273(02)00306-2 (2003).

16. Vargas, C. A. et al. Breathing of the Nevado del Ruiz volcano reservoir, Colombia, inferred from repeated seismic tomography. Sci. Rep. 7, 46094. https://doi.org/10.1038/srep46094 (2017).

17. Herring, T. A., King, R. W., Floyd, M. A., & McClusky, S. C. Introduction to GAMIT/GLOBK, Release 10.6. Massachusetts Institute of Technology, Cambridge. http://geoweb.mit.edu/gg/Intro_GG.pdf (2015).

18. Mora-Páez, H. et al. Space geodesy infrastructure in Colombia for geodynamics research. Seismol. Res. Lett. 89(2A), 446–451. https://doi.org/10.1785/0220170185 (2018).

19. McClusky, S. et al. Global positioning system constraints on plate kinematics and dynamics in the eastern Mediterranean and Caucasus. J. Geophys. Res. 105(b3), 5695–5719. https://doi.org/10.1029/1999JB900351 (2000).

20. Battaglia, M., Cervelli, P. & Murray, J. R. dMODELS: A MATLAB software package for modeling crustal deformation near active faults and volcanic centers. J. Volcanol. Geotherm. Res. 254, 1–4. https://doi.org/10.1016/j.jvolgeores.2012.12.018 (2013).

21. Williams, C. A. & Wadge, G. The effects of topography on magma chamber deformation models: Application to Mt. Etna and radar interferometry. Geophys. Res. Lett. 25–10, 1549–1552. https://doi.org/10.1029/98GL01136 (1998).

22. Lisowski, M. Analytical volcano deformation source models. In Volcano Deformation. Springer Praxis Books (ed. Dzurisin, D.) (Springer, 2007). https://doi.org/10.1007/978-3-540-49302-0_8.

23. McTigue, D. F. Elastic stress and deformation near a finite spherical magma body: Resolution of the point source paradox. J. Geophys. Res. 92, 12931–12940. https://doi.org/10.1029/JB092iB12p12931 (1987).

24. Yang, X.-M., Davis, P. M. & Dieterich, J. H. Deformation from inflation of a dipping finite prolate spheroid in an elastic half-space as a model for volcanic stressing. J. Geophys. Res. 93-B5, 4249–4257. https://doi.org/10.1029/JB093iB05p04249 (1988).

25. Fialko, Y., Khazan, Y. & Simons, M. Deformation due to a pressurized horizontal circular crack in an elastic half-space, with applications to volcano geodesy. Geophys. J. Int. 146, 181–190. https://doi.org/10.1046/j.1365-246X.2001.00452.x (2001).

26. Okada, Y. Surface deformation due to shear and tensile faults in a half-space. Bull. Seismol. Soc. Am. 75, 1135–1154. https://doi.org/10.1785/BSSA0750041135 (1985).

27. Battaglia, M. (2024). Geodetic Monitoring of the Recent Activity and the Dome Forming Eruption at Nevado del Ruiz (Colombia), 2010-2023 (1.1.0) [Data set and software]. https://doi.org/10.5281/zenodo.12194034.

## Acknowledgements

## Author contributions

Conceptualization, manuscript writing, review, and editing: M.O., J.I., and M.B. Data collection and processing: M.O., J.I., and R.A. Modelling and interpretation: M.O., J.I., and M.B. Software: M.B. Analysis of observations, and interpretation: M.O., J.I., and M.B.

## Competing interests

The authors declare no competing interests.

## Additional information

**Supplementary Information** The online version contains supplementary material available at https://doi.org/10.1038/s41598-024-72058-y.

**Correspondence** and requests for materials should be addressed to M.O.

**Reprints and permissions information** is available at www.nature.com/reprints.

**Publisher's note** Springer Nature remains neutral with regard to jurisdictional claims in published maps and institutional affiliations.